[Project Report]
Date: May 30, 2023

New Exploratory Research (Project No.: 2022H-04)

To the Director of the Disaster Prevention Research Institute, Kyoto University,

Applicant (Principal Investigator)
Name: Shengshan Wu
Position: PhD Student
Affiliation: Graduate School of Science, Kyoto University

The results of the collaborative research are reported as follows.

Project title: Unravelling the effect of rock pulverization during sliding on the hypermobility of rock avalanches: multiple approaches based experimental studies
Principal Investigator: Shengshan Wu
Affiliation: Graduate School of Science, Kyoto University
Name of DPRI CP (contact person): Gonghui WANG
Research period: 04.01, 2022 ~ 03.31, 2023
Research location: Research Center on Landslides (Laboratory: S-115D and S-116D)
Number of participants in the collaborative research: 2 (DPRI: 1 non-DPRI: 1)

Anticipated impact on research and education

Many kinds of assumptions have been proposed to explain the hypermobility of rock avalanches and the movement mechanism, but there is less evidence from tests showing that rock pulverization contributes to shear behavior. This study provides some valuable results and insight to improve understanding of the effect of rock pulverization on the shear behavior of particle materials, which can also help to enhance understanding of rock avalanches hypermobility.

Research report
(1) Purpose

Rock avalanches are a common geological disaster caused by the sudden failure of large-volume rocks that slide a long distance at an extremely fast velocity. With hypermobility, rock avalanches can travel faster and farther than normal landslides, and the apparent friction coefficient of rock avalanches is ultra-low. Recently, some field investigations indicated that rock pulverization can strongly occur during sliding. However, the effect of rock pulverization on the shear behavior of the shear surface and its implication on the hypermobility of rock avalanches is not clear. This research aims to unravel the effect of rock pulverization during sliding on the hypermobility of rock avalanches.

(2) Summary of research progress

Different shapes of halloysite nanoparticles, glass bead particles, and rice particles were used for ring shear tests. The mixture of silica sand No.8 with different content of nano silica powder was also used.

All the ring shear tests were performed with dry test conditions by ring shear apparatus DPRI-5 and DPRI-6. We employed a shear-velocity-controlled method (the maximum shear velocity is 2.24 m/s) to examine the shear stress of the samples at residual state in varying shear rate levels. Summarize the test results and check the rate effect phenomenon of the samples.

(3) Summary of research findings

I. Shear tests at high shear velocity (the maximum shear velocity is 2.24 m/s) revealed that halloysites have a strong negative rate effect, in which dehydration developed within the materials during high-speed shearing may play a contributing factor in the shear stress weakening.

II. By comparing the shear test results on nano silica powder obtained under the same test conditions, there is no rate effect phenomenon during tests, and we infer that the difference in particle shape is the possible factor for the weakening of shear strength.

III. Test results with glass beads (hardly break during tests) show that differences in particle shape lead to different shear behavior. In our tests, irregular glass beads have higher shear strength in high shear velocity (10 cm/s) than spherical glass beads.

IV. Similar results were obtained on rice particles with different shapes. The test results of long-grain rice showed a larger stress drop and lower shear strength during shearing than those of short-grain rice.

(4) Publications of research findings

- Shengshan WU, Gonghui WANG. (May 2022): Shear rate-dependent frictional properties of nanomaterials and implication for high mobility of rock avalanches, Japan Geoscience Union Meeting 2002, H-DS07-14.
- Shengshan WU, Gonghui WANG. (September 2022): Strength weakening phenomenon of nanomaterials in high-speed ring shear tests, 2022 Annual Meeting in Fukuoka, The Japan Landslide Society, P-24.
- Shengshan WU, Gonghui WANG. (November 2022): On the shear behavior of nanomaterials and its implication to landslide hypermobility, サイエンス倶楽部デイ 2022, Kyoto University, MO-16.
- Shengshan WU, Gonghui WANG. (February 2023): The effect of particle shape on the shear behavior: Results of tests on rice particles and implication, 2023 DPRI Annual Meeting, Kyoto University, D201.

The main report is as follows.

Unravelling the effect of rock pulverization during sliding on the hypermobility of rock avalanches: multiple approaches based experimental studies

1. Introduction

Rock avalanche is one of nature's most prevalent geological disasters, and it is normally characterized by its large volume, high velocity, and extremely long sliding displacement (Heim, 1932; Legros, 2002; Lucas et al., 2014; Pudasaini & Miller, 2013). Since the Elm rock avalanche was reported in detail as the first case (Hsü et al., 1978), the issue of rock avalanches has received more and more attention. In known cases, the Blackhawk landslide ran out 9 km at 235 km/h and drop 1200 m (Friedmann et. al., 2006) and the Frank slide can move at the maximal speed is about 30 m/s which occurred in April 1903 (Benko and Stead, 1998). Rock avalanches like these introduced are different from normal landslides in that they can slide faster and farther. Moreover, they took place suddenly without warning or noticeable precursors, so they caused unpredictable property losses and casualties (Delaney & Evans, 2015; Mitchell et al., 2020; Xu et al., 2012). Such as after the 2000 Yigong rock avalanche in China occurred, it caused a series of subsequent geological disasters (Zhou et al., 2016). And the Huascaran rock avalanche destroyed a town named Yungay (Mergili et al. 2018). Due to the difficulties in conducting countermeasures, to prevent or at least mitigate the possible disaster resulting from rock avalanches, better understanding their initiation and movement mechanisms will be of great importance.

Until now, researchers have been working hard for many years to better understand the mechanisms behind the high mobility of rock avalanches. After conducting numerous field investigations, Heim proposed an apparent friction coefficient value (known as Heim's ratio) to describe the high mobility of rock avalanches. Heim's ratio is calculated as the ratio of the vertical drop height of the sliding rock mass to its horizontal movement distance (Heim, 1932). Previous research indicated that Heim's ratio has an inverse relationship with the volume of the rock avalanche, with larger volumes resulting in lower Heim's ratios (Corominas, 1996; Legros, 2002; Lucas et al., 2014; Mitchell et al., 2020). In recent years, several possible assumptions have been put forth to explain the phenomenon of high mobility of rock avalanches. Such as air lubrication (Shreve, 1968), self-lubrication by transformed rock (Campbell, 1989; Erismann, 1979), lubrication by undrained loading of saturated substrates (Sassa, 1988, Wang et al., 2014), acoustic fluidization (Melosh, 1979, 1996), mechanical fluidization (McSaveney, 1978; Davies, 1982), dynamic rock fragmentation (Davies & McSaveney, 1999) and others inspired by fault tribology, frictional melt lubrication (Di Toro et al., 2006; Hirose & Shimamoto, 2005), silica-gel lubrication (Di Toro et al., 2004), powder lubrication (Reches & Lockner, 2010), flash heating (Goldsby & Tullis, 2011), and nanomaterials lubrication (Han et al., 2011). Due to the fact that most of them lack quantitative field or experimental evidence, there is no conclusive one that had been accepted widely yet.

Recently, some researchers investigate rock avalanches deposits and found the inverse grading phenomenon as one of the basic characteristics, which indicated that rock pulverization can strongly occur during sliding (Reznichenko et al., 2011; Zhang et al., 2016; McSaveney & Hu, 2022; Dufresne et al., 2016; Dufresne, 2017). However, the effect of rock pulverization on the shear behavior of the shear surface and its implication on the hypermobility of rock avalanches is not clear. In addition to reducing the size of rock particles, rock pulverization should also consider the impact of shape changes on the mobility of rock avalanches. For the purpose of this research, we performed a series of ring shear tests to investigate the effect of rock pulverization (particle size and shape) during sliding on the high mobility of rock avalanches. These findings could provide valuable insights into the effect of particle characterization on shear behavior.

2. Materials and methods

The ring shear test has the advantage of being able to shear with infinite displacement, and it is a widely used method for evaluating the residual resistance of materials (Bishop et al., 1971; Sassa, 1988). In this research, we used ring shear apparatuses (DPRI-5 and DPRI-6) as shown in Figure 1 developed at Kyoto University (Sassa et al., 2004). DPRI-5 has a 12cm inner diameter and an 18 cm outer diameter, while the shear box of DPRI-6 is a 25 cm inner diameter and a 35 cm outer diameter (Sassa et al., 2004). All ring shear tests were performed by controlling the shear velocity from low to high speed. It is noticed that the available maximum shear velocities for DPRI-5 and DPRI-6 are 10.0 cm/s and 224 cm/s, respectively.

Our primary objective was to gather scientific evidence and determine the potential implications of the high mobility observed in rock avalanches. To accomplish this, we focused on investigating the influence of particle characteristics, specifically size and shape, on the shear behavior of these avalanches. In order to isolate and analyze these factors, all ring shear tests were conducted under dry conditions. This approach allowed us to closely examine the effect of particle size and shape on the movement and shear behavior of particle materials, without the confounding influence of external factors such as water content or pore pressure. There are four types of materials as samples are used in this study. Including different shapes of halloysite nanoparticles, glass bead particles, rice particles, and the mixture of silica sand No.8 with different content of nano silica powder. Figure 2 shows the shape and size characteristics of each type of sample. In addition, in order to facilitate the comparison of test results conducted under different stress conditions, the stress ratio (Stress ratio = shar resistance / normal stress) was used to evaluate changes in shear stress. Table 1 shows the ring shear tests performed.

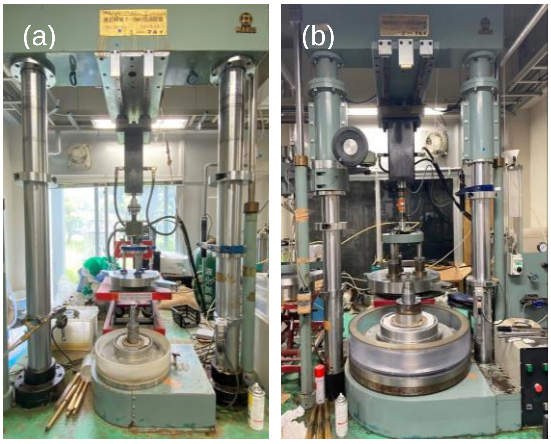

Fig. 1. Ring shear apparatuses: a. DPRI-5; b. DPRI-6

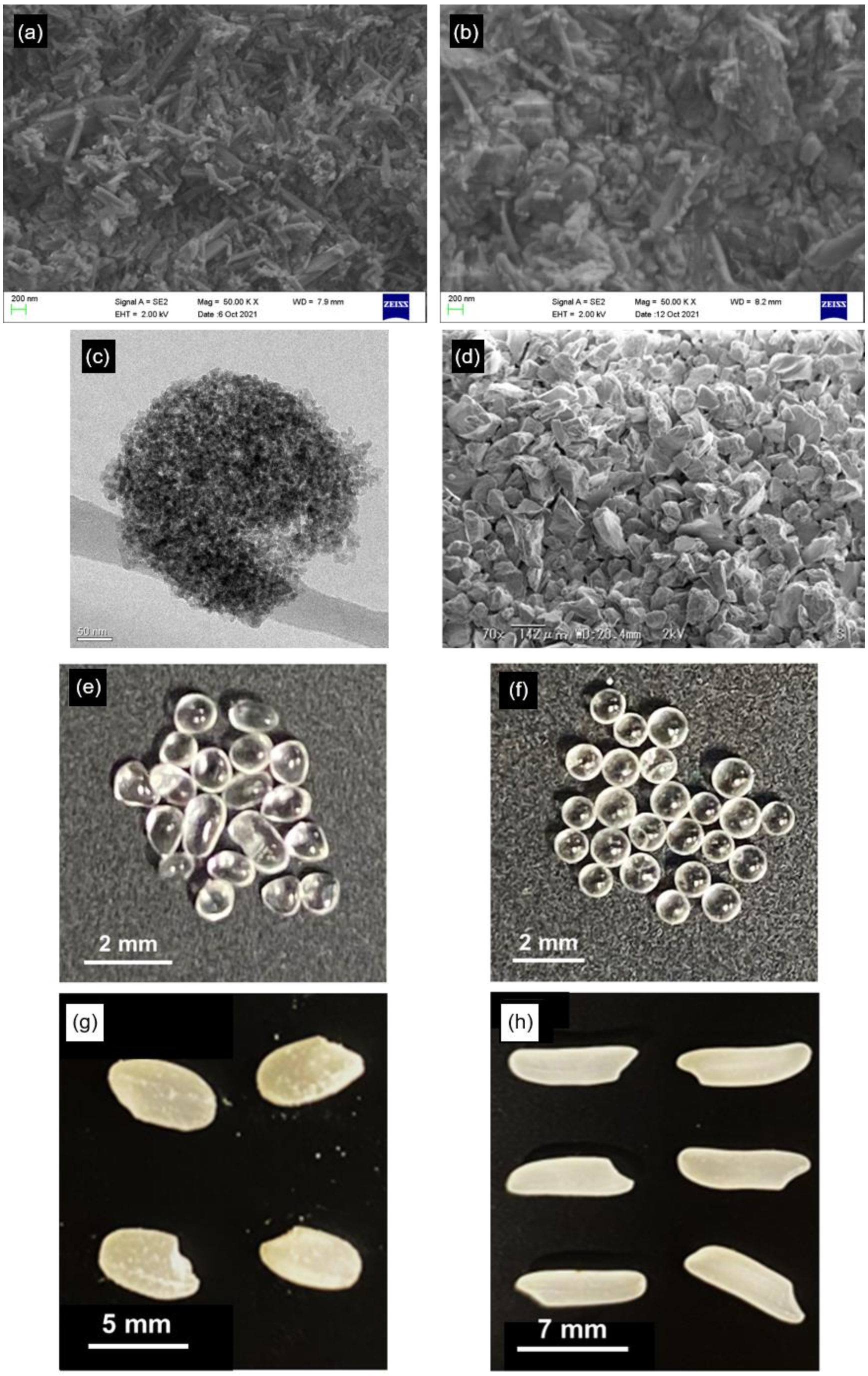

Fig. 2. Samples for ring shear tests: a. halloysite from American Dragon (ADH); b. halloysite from New Zealand (NZH); c. nano silica (SN); d. silica sand no. 8 (S8); e. raindrops-like glass beads (GBI); f. spherical glass beads (GBS); g. short-grain rice particles (RJ); h. long-grain rice particles (RT).

Table 1. Ring shear tests conditions

Sample	Sample shape	Sample size	Normal stress	Shear velocity	Remarks
Halloysite					
ADH-N	Tube	Nanoscale	200 kPa	0 ~ 2 m/s (approximately)	Shown in Fig. 3a
ADH-500	Tube	Nanoscale	200 kPa	0 ~ 2 m/s (approximately)	Shown in Fig. 3b
NZH-N	A mixture of tube and spheroid	Nanoscale	200 kPa	0 ~ 2 m/s (approximately)	Shown in Fig. 3c
NZH-500	A mixture of tube and spheroids	Nanoscale	200 kPa	0 ~ 2 m/s (approximately)	Shown in Fig. 3d
Mixtures of nano silica (SN) and silica sand no. 8 (S8)					
M0	Subangular to angular particles	D_{50}≈0.12	150 kPa	0.1 ~ 20 cm/s	Shown in Fig. 6a
M10	Undefined	Undefined	150 kPa	0.1 ~ 20 cm/s	Shown in Fig. 6b
M20	Undefined	Undefined	150 kPa	0.1 ~ 20 cm/s	Shown in Fig. 6c
M50	Undefined	Undefined	150 kPa	0.1 ~ 20 cm/s	Shown in Fig. 6d
Glass beads					
GBI_{08}	Raindrops-like	0.85 ~ 1.18 mm	150 kPa	0.005 ~ 10 cm/s	Shown in Fig. 8
GBS_{08}	Spheroid	0.85 ~ 1.18 mm	150 kPa	0.005 ~ 10 cm/s	Shown in Fig. 9
Rice particles		0.85 ~ 1.18 mm			
RJ	Short-grain	0.85 ~ 1.18 mm	42 kPa	0.01 ~ 10 cm/s	Shown in Fig. 11
RT	Long-grain	0.85 ~ 1.18 mm	43 kPa	0.02 ~ 10 cm/s	Shown in Fig. 12

Note: normal halloysite from American Dragon (ADH-N); ADH was dried at 500 ℃ (ADH-500); normal halloysite from New Zealand (NZH-N); NZH was dried at 500 ℃ (NZH-500); M0 corresponds to pure S8, M10, M20, and M50 to mixtures of S8 with 10, 20, and 50% of SN by weight, respectively.

3. Results

3.1. Ring shear results on halloysite

For each test on halloysite, we controlled the shear velocity from 0 to 2 m/s and then gradually decreased until it stopped. Figure 3 shows the results of ring shear tests on different types of halloysite and similar shear behavior should be found. For example, as shown in Figure 3a, AHD-N was first sheared at a low shear velocity until about 0.1 m. At this stage, the stress ratio is kept at about 0.7, and it is considered that the shear zone has been formed. In the subsequent stages of shearing, the shearing velocity was systematically increased to approximately 2 m/s. As the shearing speed increased, we observed a gradual decrease in the stress ratio, reaching its lowest value at approximately 0.2. It is a typical rate-effect phenomenon during the test. Similar phenomena were also found in several other ring shear tests (figures. 3b-3d). In every test, the stress ratio was reduced to a minimum when the shear velocity was maximized.

Due to halloysite being a kind of material that could be easily dehydrated (figure. 4), we examined the shear behavior of samples (ADH-D500 and NZH-D500) that were pre-dried at 500 ℃ for 24 h (figures. 3b and 3d). It can be found that the stress ratios of the dried samples (ADH-D500 and NZH-D500) were slightly higher than those of the normal samples (ADH-N and NZH-N) when shearing the samples at the maximum speed, respectively. And the results indicate that in our tests, the dehydration of the samples during the shear process can contribute to the weakening trend of the shear resistance. We also found in Figure 4 that the stress ratio of tube shape halloysite is lower than that of the mixed-shaped one (ADH-D＜NZH-N; ADH-N500＜NZH-N500) at max shear velocity. That is to say, the difference in sample shape is also a key factor for the weakening of shear resistance in this study.

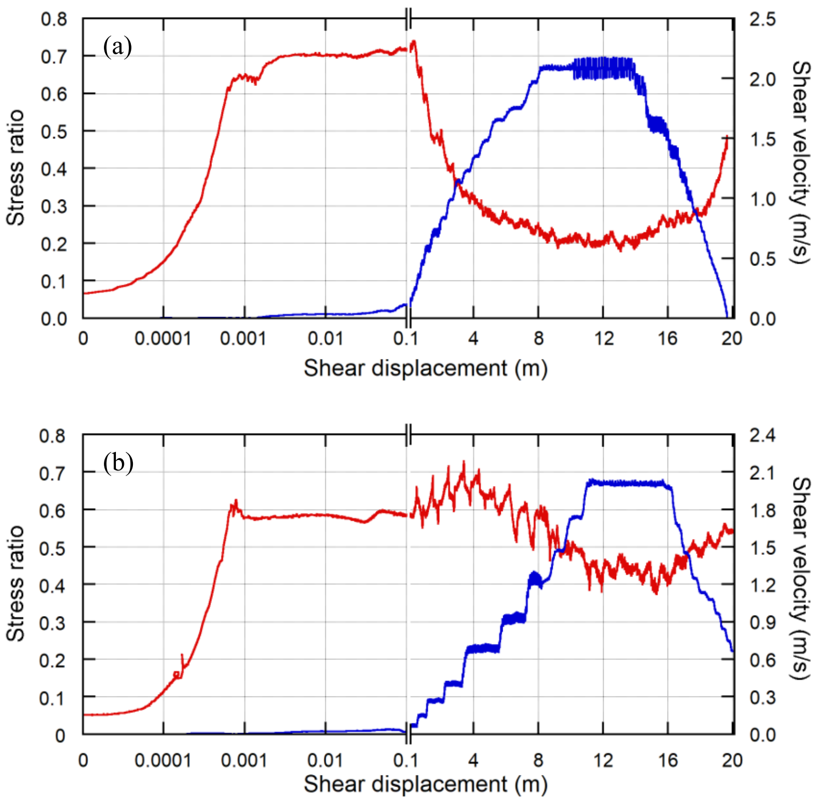

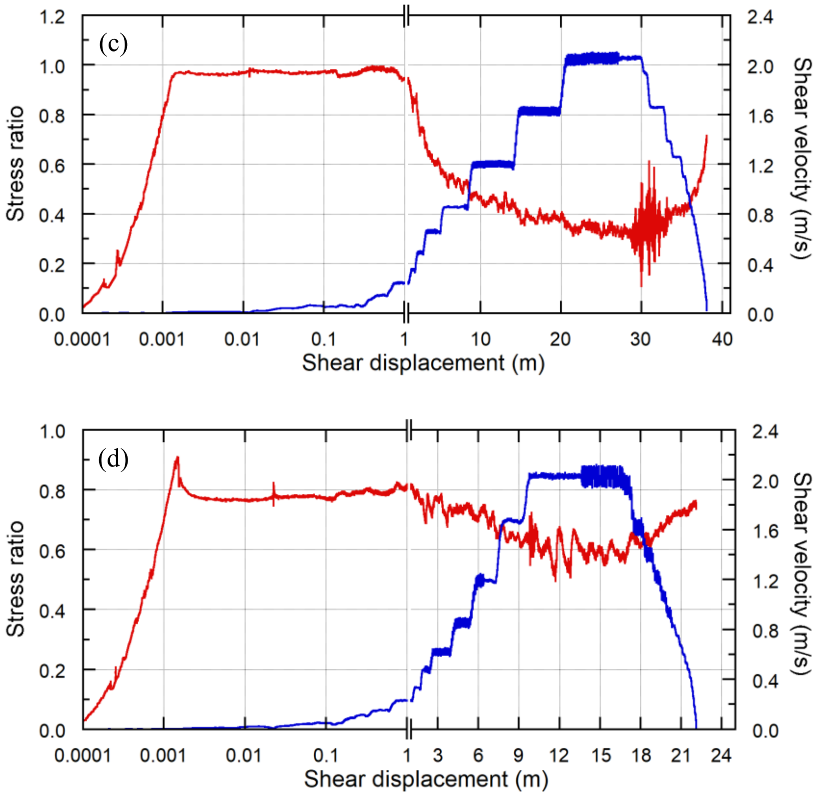

Fig. 3. Results of high shear-velocity ring shear tests on different types of halloysite: (a) AHD-N, (b) AHD-500, (c) NZH-N, (d) NZH-500.

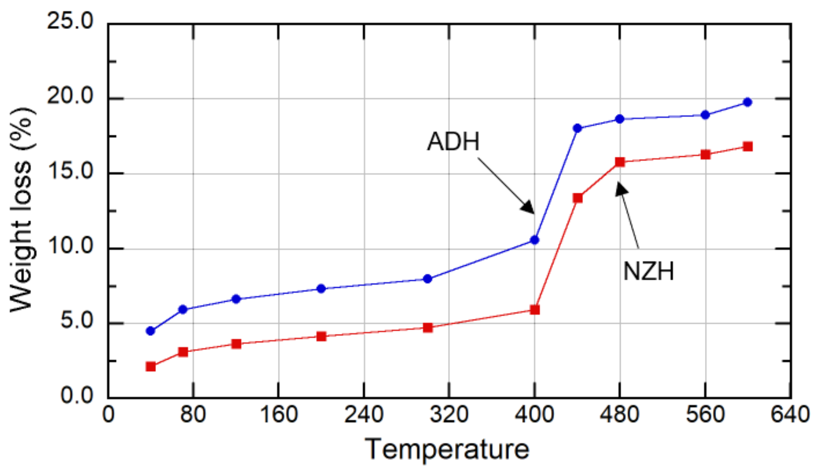

Fig. 4. Weight loss curve of halloysite

3.2. Ring shear results on mixtures of nano silica and silica sand no. 8

Figure. 5 shows the shear behavior of SN at high shear velocity. There is no found rate effect phenomenon during the test, the stress ratio of SN keeps around 0.6, even though when shear velocity arrives at about 2 m/s. Figure. 6 presented stress ratio curves obtained from ring shear tests conducted at different shear velocities, including tests conducted on mixed samples of S8 and various SN contents (M0, M10, M20, M50). In Figure. 6a, for example, S8 was sheared at shear velocities ranging from 0.1

cm/s to 20 cm/s. At each shear velocity level, the sample was sheared at least one circle before switching to the next shear velocity. The stress ratio curve does not present data during the acceleration stage. Throughout the testing process, S8 exhibited relatively stable shear behavior at different shear rates, with a stress ratio of around 0.62, indicating that S8 is a granular material without rate effect (Hunger & Morgenstern, 1984). The same method was used to test the shear behavior of the mixed samples after adding different SN contents to S8, and the results are shown in Figures. 6b-6d. We compared the mean value of the stress ratio at different shear velocity levels of these ring shear tests (Fig. 7) and found that when the SN content of the mixed sample was low (M10 and M20 in this research), the stress ratio was higher than that of S8. On the other hand, when the SN content was high, the stress ratio was slightly lower than that of S8. Nevertheless, as increasing of shear velocity, the stress ratio kept relatively stable for each test respectively. Stress ratio and nanoparticle content do not have a positive correlation.

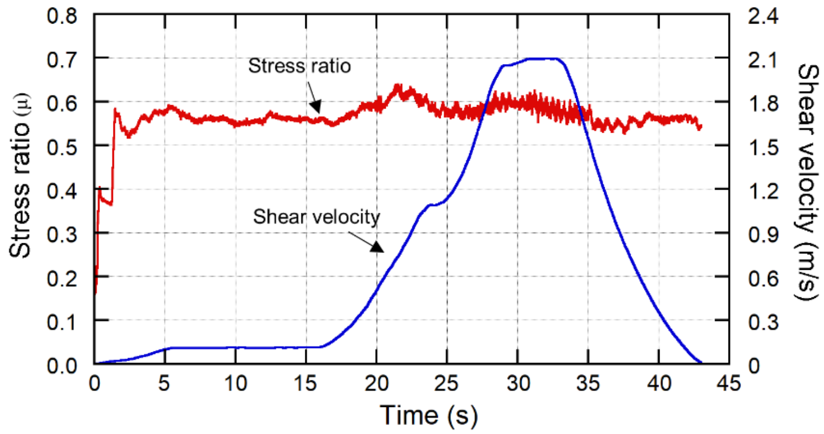

Fig. 5. Result of high shear-velocity ring shear test on SN

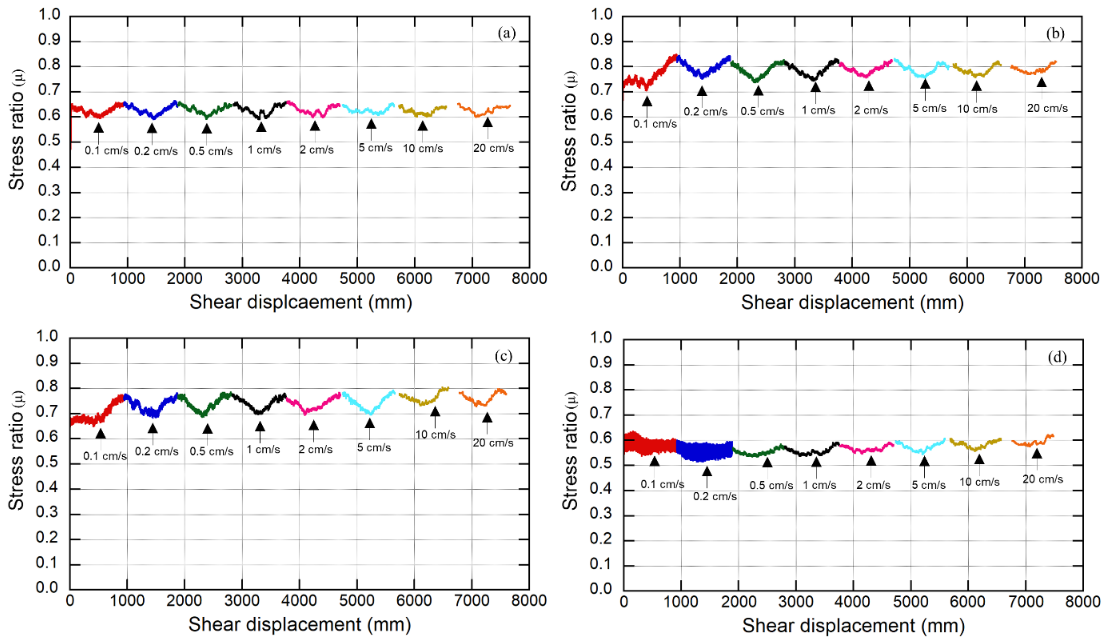

Fig. 6. Results of ring shear tests on SN and S8 mixture: (a) M0, (b) M10, (c) M20, (d) M50.

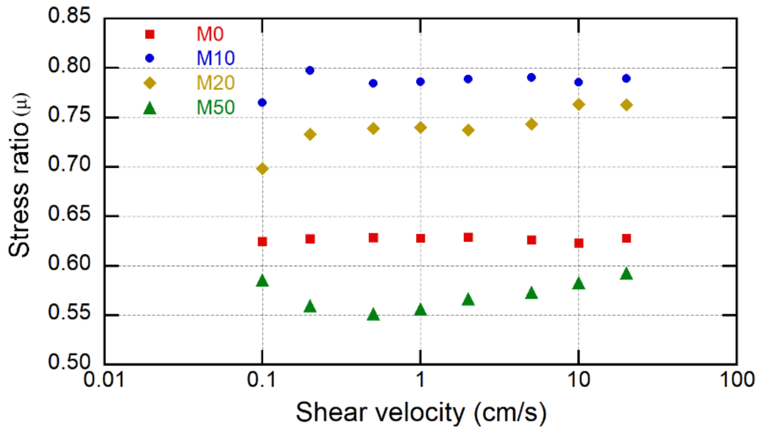

Fig. 7. Changes of steady-state mean stress ratio with shear velocity.

3.3. Ring shear results on glass beads

In order to further study the effect of particle shape on shear behavior, we selected glass beads with approximately the same size and different shapes (spheroid and raindrop-like) for ring shear tests. Glass beads have stable properties and are suitable for our research purposes. Figures 8 and 9 show the shear behavior of spherical (GBS) and raindrop-like glass beads (GBI), respectively. Similarly, as the shear velocity increases, the shear mode of the sample changes from stick-slip to stable sliding, and the shear resistance decreases gradually. It can be seen from Figure 10 that although the stress ratio of GBI varies greatly, the stress ratio of GBS is smaller than that of GBI at all shear velocity levels.

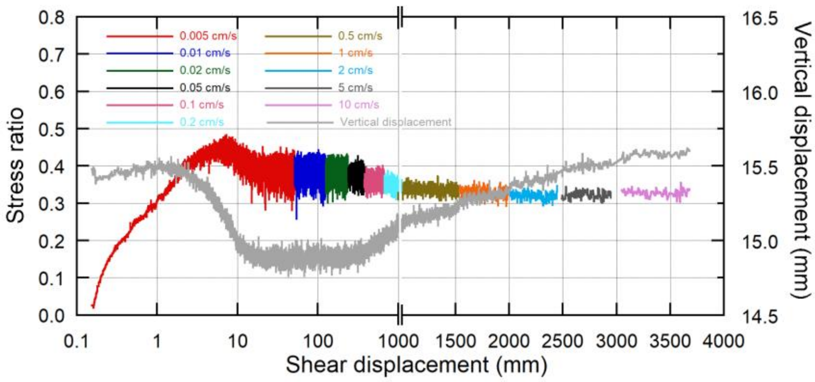

Fig. 8. Results of ring shear test on GBS

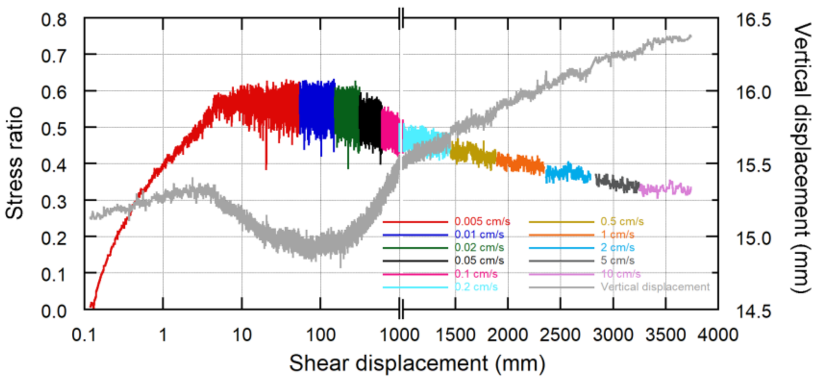

Fig. 9. Results of ring shear test on GBI

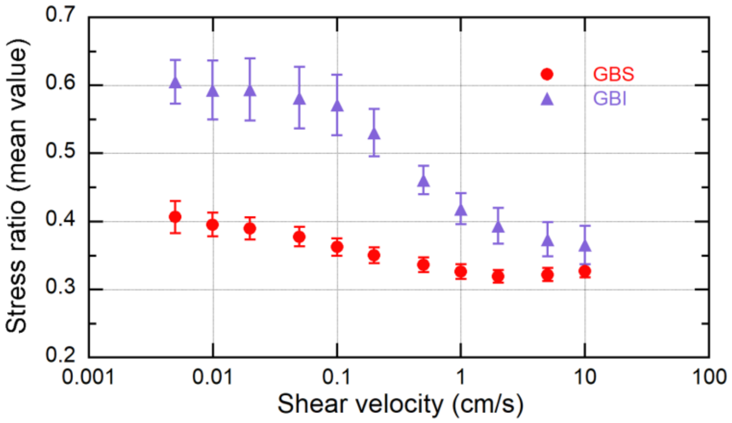

Fig. 10. The comparison of ring shear test results of RJ and RT

3.4. Ring shear results on rice particles

After examining different shapes of rice (RT and RJ), the shearing results showed similar shearing behavior as glass beads. At relatively low shear velocity, stronger stick-slip phenomena are easily found in the results (Figures. 11 and 12). However, as the shear velocity increases, the shear resistance of samples weakens. Also, the stress ratio of RJ is lower than that of RT (Figure. 13). But based on the present data and thinking, we still could not explain well why the stress ratio of RT is lower than that of RJ at the shear velocity of 5 and 10 cm/s. We surmise that this is due to the obvious difference in the size of the two shapes of rice grains. Another possibility is that even if we use low normal stress to examine the rice particles, there will still be a small number of particles that occurred breakage during tests. Both of these factors may contribute to differences in shear behavior.

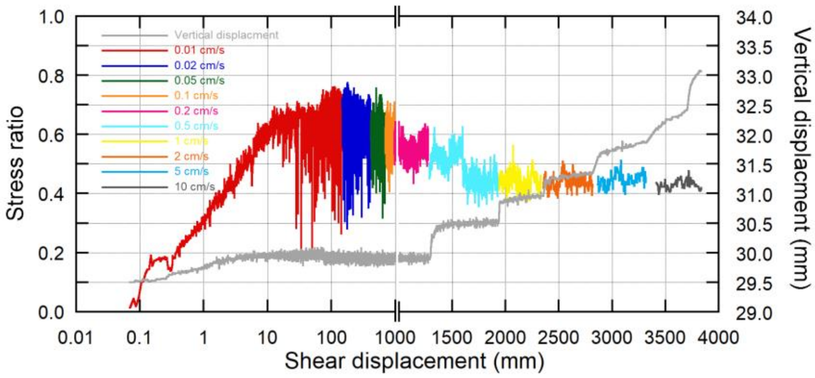

Fig. 11. Results of ring shear test on RJ

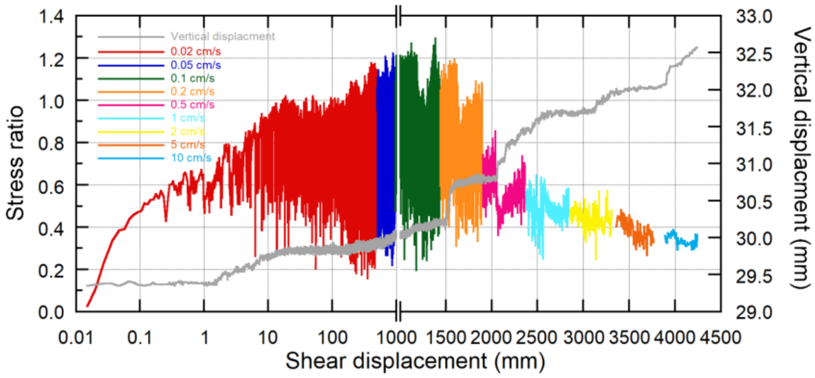

Fig. 12. Results of ring shear test on RT

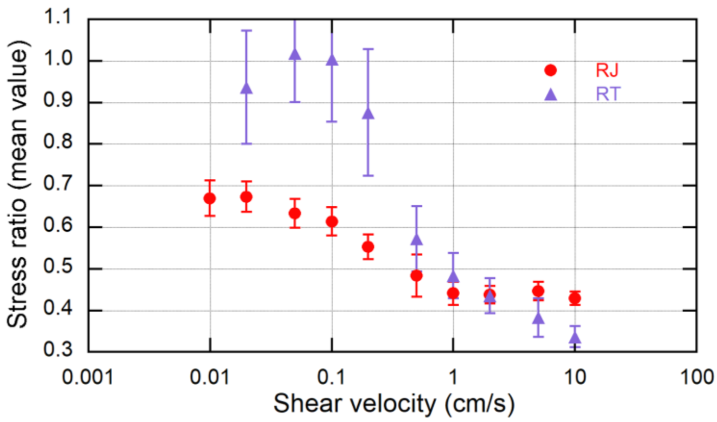

Fig. 13. The comparison of ring shear test results of RJ and RT

4. Summary

In this research, in order to unravel the effect of rock pulverization during sliding on hypermobility, a series of dry ring shear tests have been performed. Based on the results introduced, the following summaries could be drawn:

I. Shear tests at high shear velocity (the maximum shear velocity is 2.24 m/s) revealed that halloysites have a strong negative rate effect, in which dehydration developed within the materials during high-speed shearing may play a contributing factor in the shear stress weakening.

II. Shear test results on nano silica powder obtained under the same test conditions, there is no rate effect phenomenon during tests, which indicates that not all the nanoparticles exhibit rate effect phenomena in high-velocity shear tests. And comparing the results with the test results of halloysite, we infer that the difference in particle shape is the possible factor for the weakening of shear strength.

III. Test results with glass beads (GBS and GBI) show that differences in particle shape lead to different shear behavior. In our tests, GBI has higher shear strength in high shear velocity (10 cm/s) than GBS.

IV. The ring shear tests on rice particles with different shapes (RJ and RT) are similar to glass beads. The test results of RT showed a larger stress drop and lower shear strength during shearing than those of RJ.

5. Future study

Research on the influence of particle shape on shear behavior continues, and we are performing a new series of ring shear tests. In the future, we hope to obtain more data and understand the mechanism more deeply.

Acknowledgments

This study is supported by the New Exploratory Research Grant (NO. 2022H-04) from Disaster Prevention Research Institute, Kyoto Univerity.

References

Bishop, A. W., Green, G. E., Garga, V. K., Andresen, A., & Brown, J. D. (1971). A new ring shear apparatus and its application to the measurement of residual strength. *Geotechnique*, 21(4), 273-328. https://doi.org/10.1680/geot.1971.21.4.273

Benko B, Stead D. The Frank slide: a reexamination of the failure mechanism[J]. Canadian Geotechnical Journal, 1998, 35(2): 299-311.

Campbell, C. S. (1989). Self-lubrication for long runout landslides. *The Journal of Geology*, 97(6), 653-665. https://doi.org/10.1086/629350.

Corominas, J. (1996). The angle of reach as a mobility index for small and large landslides. *Canadian Geotechnical Journal*, *33*(2), 260–271. https://doi.org/10.1139/t96-005.

Davies, T.R.H. (1982). The spreading of rock avalanche debris by mechanical fluidization. *Rock Mechanics*, 15: 9–24. https://doi.org/10.1007/BF01239474.

Davies, T. R., & McSaveney, M. J. (1999). Runout of dry granular avalanches. *Canadian Geotechnical Journal*, *36*(2), 313–320. https://doi.org/10.1139/t98-108.

Delaney, K. B., & Evans, S. G. (2015). The 2000 Yigong landslide (Tibetan Plateau), rockslide-dammed lake and outburst flood: Review, remote sensing analysis, and process modelling. *Geomorphology*, 246, 377-393. https://doi.org/10.1016/j.geomorph.2015.06.020.

Di Toro, G., Goldsby, D. L., & Tullis, T. E. (2004). Friction falls towards zero in quartz rock as slip velocity approaches seismic rates. Nature, 427(6973), 436–439. https://doi.org/10.1038/nature02249

Di Toro, G., Han, R., Hirose, T., De Paola, N., Nielsen, S., Mizoguchi, K., Ferri, F., Cocco, M., & Shimamoto, T. (2011). Fault lubrication during earthquakes. *Nature*, 471(7339), 494-498. https://doi.org/10.1038/nature09838.

Di Toro, G., Hirose, T., Nielsen, S., Pennacchioni, G., & Shimamoto, T. (2006). Natural and experimental evidence of melt lubrication of faults during earthquakes. *Science*, *311*(5761), 647–649. https://doi.org/10.1126/science.1121012.

Dufresne A. Rock avalanche sedimentology—recent progress[J]. Advancing Culture of Living with Landslides: Volume 2 Advances in Landslide Science, 2017: 117-122.

Dufresne A, Bösmeier A, Prager C. Sedimentology of rock avalanche deposits–case study and review[J]. Earth-Science Reviews, 2016, 163: 234-259. https://doi.org/10.1016/j.earscirev.2016.10.002.

Erismann, T. H. (1979). Mechanisms of large landslides. Rock Mechanics, 12(1), 15-46. Mechanisms of large landslides. *Rock Mechanics 12*(1), 15–46. https://doi.org/10.1007/BF01241087.

Friedmann S J, Taberlet N, Losert W. Rock-avalanche dynamics: insights from granular physics experiments[J]. International Journal of Earth Sciences, 2006, 95: 911-919.

Goldsby, D. L., & Tullis, T. E. (2011). Flash heating leads to low frictional strength of crustal rocks at earthquake slip rates. *Science*, *334*(6053), 216–218. https://doi.org/10.1126/science.1207902.

Han, R., Hirose, T., & Shimamoto, T. (2010). Strong velocity weakening and powder lubrication of simulated carbonate faults at seismic slip rates. *Journal of Geophysical Research: Solid Earth*, *115*(B3). https://doi.org/10.1029/2008JB006136.

Han, R., Hirose, T., Shimamoto, T., Lee, Y., & Ando, J. I. (2011). Granular nanoparticles lubricate faults during seismic slip. *Geology*, *39*(6), 599–602. https://doi.org/10.1130/G31842.1.

Heim, A., (1932) Bergsturz und Menschleben. Fretz and Wasmuth, Zurich. 218 pp.

Hirose, T., & Shimamoto, T. (2005). Growth of molten zone as a mechanism of slip weakening of simulated faults in gabbro during frictional melting. *Journal of Geophysical Research: Solid Earth*, 110(B5). https://doi.org/10.1029/2004JB003207.

Hsü, K. J., & Voight, B. (1978). Albert Heim: observations on landslides and relevance to modern interpretations. *Natural Phenomena*, 1, 70-93.

Hungr, O., & Morgenstern, N. R. (1984). High velocity ring shear tests on sand. *Geotechnique*, 34(3), 415-421. https://doi.org/10.1680/geot.1984.34.3.415.

Legros, F. (2002). The mobility of long-runout landslides. *Engineering Geology*, *63*(3–4), 301–331. https://doi.org/10.1016/S0013-7952(01)00090-4.

Lucas, A., Mangeney, A., & Ampuero, J. P. (2014). Frictional velocity-weakening in landslides on Earth and on other planetary bodies. *Nature communications*, 5(1), 1-9. https://doi.org/10.1038/ncomms4417.

McSaveney, M. J. (1978). "Sherman glacier rock avalanche, Alaska, USA." *Developments in Geotechnical Engineering*. Vol. 14, pp. 197-258.

McSaveney, M., & Hu, W. (2022). Nanoparticles in the 2008 Yangjiagou rock avalanche. Short Papers and Extended Abstracts, Geological Society of America Penrose Conference Penrose Conference: Progressive Failure of Brittle Rocks. PRF2022. Flat Rock, N.C., 20-24 June, 2022. https://doi.org/10.1130/abs/2022PR-376041.

Melosh, H. J. (1979). Acoustic fluidization: a new geologic process? *Journal of Geophysical Research*, *84*(B13), 7513–7520. https://doi.org/10.1029/JB084iB13p07513.

Melosh, H. J. (1996). Dynamical weakening of faults by acoustic fluidization. *Nature*, *379*(6566), 601–606. https://doi.org/10.1038/379601a0.

Mergili M, Frank B, Fischer J T, et al. Computational experiments on the 1962 and 1970 landslide events at Huascarán (Peru) with r. avaflow: Lessons learned for predictive mass flow simulations[J]. Geomorphology, 2018, 322: 15-28.

Mitchell, A., McDougall, S., Aaron, J., & Brideau, M. A. (2020). Rock avalanche-generated sediment mass flows: Definitions and hazard. *Frontiers in Earth Science*, 8, 543937.

https://doi.org/10.3389/feart.2020.543937.

Pudasaini, S. P., & Miller, S. A. (2013). The hypermobility of huge landslides and avalanches. *Engineering Geology*, *157*, 124–132. https://doi.org/10.1016/j.enggeo.2013.01.012.

Reches, Z., & Lockner, D. A. (2010). Fault weakening and earthquake instability by powder lubrication. *Nature*, *467*(7314), 452–455. https://doi.org/10.1038/nature09348.

Reznichenko N V, Davies T R H, Alexander D J. Effects of rock avalanches on glacier behaviour and moraine formation[J]. Geomorphology, 2011, 132(3-4): 327-338. https://doi.org/10.1016/j.geomorph.2011.05.019.

Sassa, K. (1988), Geotechnical model for the motion of landslides, in Proceedings of the 5th International Symposium on Landslides, pp. 37–55, Lausanne, Switzerland.

Sassa, K., Fukuoka, H., Wang, G., & Ishikawa, N. (2004). Undrained dynamic-loading ring-shear apparatus and its application to landslide dynamics. *Landslides*, *1*(1), 7–19. https://doi.org/10.1007/s10346-003-0004-y.

Shreve, R. L. (1968). Leakage and fluidization in air-layer lubricated avalanches. *The Geological Society of America Bulletin*, 79(5), 653–658. https://doi.org/10.1130/0016-7606(1968)79[653:lafial]2.0.co;2

Wang, G., Huang, R., Lourenço, S. D., & Kamai, T. (2014). A large landslide triggered by the 2008 Wenchuan (M8. 0) earthquake in Donghekou area: Phenomena and mechanisms. *Engineering Geology*, 182, 148-157. https://doi.org/10.1016/j.enggeo.2014.07.013.

Xu, Q., Shang, Y., van Asch, T., Wang, S., Zhang, Z., & Dong, X. (2012). Observations from the large, rapid Yigong rock slide–debris avalanche, southeast Tibet. *Canadian Geotechnical Journal*, 49(5), 589-606. https://doi.org/10.1139/t2012-021.

Zhang M, Yin Y, McSaveney M. Dynamics of the 2008 earthquake-triggered Wenjiagou Creek rock avalanche, Qingping, Sichuan, China[J]. Engineering Geology, 2016, 200: 75-87. https://doi.org/10.1016/j.enggeo.2015.12.008

Zhou J, Cui P, Hao M. Comprehensive analyses of the initiation and entrainment processes of the 2000 Yigong catastrophic landslide in Tibet, China[J]. Landslides, 2016, 13: 39-54.